

Stochastic Video Generation with a Learned Prior

Emily Denton¹ Rob Fergus^{1,2}

Abstract

Generating video frames that accurately predict future world states is challenging. Existing approaches either fail to capture the full distribution of outcomes, or yield blurry generations, or both. In this paper we introduce an unsupervised video generation model that learns a prior model of uncertainty in a given environment. Video frames are generated by drawing samples from this prior and combining them with a deterministic estimate of the future frame. The approach is simple and easily trained end-to-end on a variety of datasets. Sample generations are both varied and sharp, even many frames into the future, and compare favorably to those from existing approaches.

1. Introduction

Learning to generate future frames of a video sequence is a challenging research problem with great relevance to reinforcement learning, planning and robotics. Although impressive generative models of still images have been demonstrated (e.g. Reed et al. (2017); Karras et al. (2017)), these techniques do not extend to video sequences. The main issue is the inherent uncertainty in the dynamics of the world. For example, when a bouncing ball hits the ground unknown effects, such surface imperfections or ball spin, ensure that its future trajectory is inherently random.

Consequently, pixel-level frame predictions of such an event degrade when a deterministic loss function is used, e.g. with the ball itself blurring to accommodate multiple possible futures. Recently, loss functions that impose a distribution instead have been explored. One such approach are adversarial losses (Goodfellow et al., 2014), but training difficulties and mode collapse often mean the full distribution is not captured well.

We propose a new stochastic video generation (SVG) model that combines a deterministic frame predictor with time-dependent stochastic latent variables. We propose two vari-

ants of our model: one with a fixed prior over the latent variables (SVG-FP) and another with a learned prior (SVG-LP). The key insight we leverage for the learned-prior model is that for the majority of the ball’s trajectory, a deterministic model suffices. Only at the point of contact does the modeling of uncertainty become important. The learned prior can be interpreted as a *predictive model of uncertainty*. For most of the trajectory the prior will predict low uncertainty, making the frame estimates deterministic. However, at the instant the ball hits the ground it will predict a high variance event, causing frame samples to differ significantly.

We train our model by introducing a recurrent inference network to estimate the latent distribution for each time step. This novel recurrent inference architecture facilitates easy end-to-end training of SVG-FP and SVG-LP. We evaluate SVG-FP and SVG-LP on two real world datasets and a stochastic variant of the Moving MNIST dataset. Sample generations are both varied and sharp, even many frames into the future.

2. Related work

Several models have been proposed that use prediction within video to learn deep feature representations appropriate for high-level tasks such as object detection. Wang & Gupta (2015) learn an embedding for patches taken from object video tracks. Zou et al. (2012) use similar principles to learn features that exhibit a range of complex invariances. Lotter et al. (2016) propose a predictive coding model that learns features effective for recognition of synthetic faces, as well as predicting steering angles in the KITTI benchmark. Criteria related to slow feature analysis (Wiskott & Sejnowski, 2002) have been proposed such as linearity of representations (Goroshin et al., 2015) and equivariance to ego-motion (Jayaraman & Grauman, 2015). Agrawal et al. (2015) learn a representation by predicting transformations obtained by ego-motion.

A range of deep video generation models have recently been proposed. Srivastava et al. (2015) use LSTMs trained on pre-learned low dimensional image representations. Ranzato et al. (2014) adopt a discrete vector quantization approach inspired by text models. Video Pixel Networks (Kalchbrenner et al., 2016) are a probabilistic approach to generation whereby pixels are generated one at a time in raster-scan or-

¹Courant Institute, New York University ²Facebook AI Research. Correspondence to: Remi Denton <denton@cs.nyu.edu>.

der (similar autoregressive image models include Salimans et al. (2017); van den Oord et al. (2016)). Our approach differs from these in that it uses continuous representations throughout and generates the new frame directly, rather than via a sequential process over scale or location.

Finn et al. (2016) use an LSTM framework to model motion via transformations of groups of pixels. Other works predict optical flows fields that can be used to extrapolate motion beyond the current frame, e.g. (Liu, 2009; Xue et al., 2016; Walker et al., 2015). Although we directly generate pixels, our model also computes local transformations but in an implicit fashion. Skip connections between encoder and decoder allow direct copying of the previous frame, allowing the rest of the model to focus on changes. However, our approach is able handle stochastic information in a more principled way.

Another group of approaches factorize the video into static and dynamic components before learning predictive models of the latter. Denton & Birodkar (2017) decomposes frames into content and pose representations using a form of adversarial loss to give a clean separation. An LSTM is then applied to the pose vectors to generate future frames. Villegas et al. (2017a) do pixel level prediction using an LSTM that separates out motion and content in video sequences. A reconstruction term is used that combines mean squared error and a GAN-based loss. Although our approach also factorizes the video, it does so into deterministic and stochastic components, rather than static/moving ones. This is an important distinction, since the difficulty in making accurate predictions stems not so much from the motion itself, but the uncertainty in that motion.

Villegas et al. (2017b) propose a hierarchical model that first generates high level structure of a video and then generates pixels conditioned on the high level structure. This method is able to successfully generate complex scenes, but unlike our unsupervised approach, requires annotated pose information at training time.

Chiappa et al. (2017) and Oh et al. (2015) focus on action-conditional prediction in video game environments, where known actions at each frame are assumed. These models produce accurate long-range predictions. In contrast to the above works, we do not utilize any action information.

Several video prediction approaches have been proposed that focus on handling the inherent uncertainty in predicting the future. Mathieu et al. (2016) demonstrate that a loss based on GANs can produce sharper generations than traditional ℓ_2 -based losses. Vondrick et al. (2016) train a generative adversarial network that separates out foreground and background generation. Vondrick & Torralba (2017) propose a model based on transforming pixels from the past and train with an adversarial loss. All these approaches

use a GAN to handle uncertainty in pixel-space and this introduces associated difficulties with GANs, i.e. training instability and mode collapse. By contrast, our approach only relies on an ℓ_2 loss for pixel-space reconstruction, having no GANs or other adversarial terms.

Other approaches address uncertainty in predicting the future by introducing latent variables into the prediction model. Henaff et al. (2017) disentangle deterministic and stochastic components of a video by encoding prediction errors of a deterministic model in a low dimensional latent variable. This approach is broadly similar to ours, but differs in the way the latent variables are inferred during training and sampled at test time. The closest work to ours is that of Babaeizadeh et al. (2017), who propose a variational approach from which stochastic videos can be sampled. We discuss the relationship to our model in more depth in Section 3.1.

Stochastic temporal models have also been explored outside the domain of video generation. Bayer & Osendorfer (2014) introduce stochastic latent variables into a recurrent network in order to model music and motion capture data. This method utilizes a recurrent inference network similar to our approach and the same time-independent Gaussian prior as our fixed-prior model. Several additional works train stochastic recurrent neural networks to model speech, handwriting, natural language (Chung et al., 2015; Fraccaro et al., 2016; Bowman et al., 2016), perform counterfactual inference (Krishnan et al., 2015) and anomaly detection (Sölch et al., 2016). As in our work, these methods all optimize a bound on the data likelihood using an approximate inference network. They differ primarily in the parameterization of the approximate posterior and the choice of prior model.

3. Approach

We start by explaining how our model generates new video frames, before detailing the training procedure. Our model has two distinct components: (i) a prediction model p_θ that generates the next frame $\hat{\mathbf{x}}_t$, based on previous ones in the sequence $\mathbf{x}_{1:t-1}$ and a latent variable \mathbf{z}_t and (ii) a prior distribution $p(\mathbf{z})$ from which \mathbf{z}_t is sampled at *each time step*. The prior distribution can be fixed (SVG-FP) or learned (SVG-LP). Intuitively, the latent variable \mathbf{z}_t carries all the stochastic information about the next frame that the deterministic prediction model cannot capture. After conditioning on a short series of real frames, the model can generate multiple frames into the future by passing generated frames back into the input of the prediction model and, in the case of the SVG-LP model, the prior also.

The model is trained with the aid of a separate inference model (not used at test time). This takes as input the frame \mathbf{x}_t ,

i.e. the target of the prediction model, and previous frames $\mathbf{x}_{1:t-1}$. From this it computes a distribution $q_\phi(\mathbf{z}_t | \mathbf{x}_{1:t})$ from which we sample \mathbf{z}_t . To prevent \mathbf{z}_t just copying \mathbf{x}_t , we force $q_\phi(\mathbf{z}_t | \mathbf{x}_{1:t})$ to be close to the prior distribution $p(\mathbf{z})$ using a KL-divergence term. This constrains the information that \mathbf{z}_t can carry, forcing it to capture new information not present in previous frames. A second term in the loss penalizes the reconstruction error between $\hat{\mathbf{x}}_t$ and \mathbf{x}_t . Fig. 1a shows the inference procedure for both SVG-FP and SVG-LP. The generation procedure for SVG-FP and SVG-LP are shown in Fig. 1b and Fig. 1c respectively.

To further explain our model we adopt the formalism of variational auto-encoders. Our recurrent frame predictor $p_\theta(\mathbf{x}_t | \mathbf{x}_{1:t-1}, \mathbf{z}_{1:t})$ is specified by a fixed-variance conditional Gaussian distribution $\mathcal{N}(\mu_\theta(\mathbf{x}_{1:t-1}, \mathbf{z}_{1:t}), \sigma)$. In practice, we set $\hat{\mathbf{x}}_t = \mu_\theta(\mathbf{x}_{1:t-1}, \mathbf{z}_{1:t})$, i.e. the mean of the distribution, rather than sampling. Note that at time step t the frame predictor only receives \mathbf{x}_{t-1} and \mathbf{z}_t as input. The dependencies on all previous $\mathbf{x}_{1:t-2}$ and $\mathbf{z}_{1:t-1}$ stem from the recurrent nature of the model.

Since the true distribution over latent variables \mathbf{z}_t is intractable we rely on a time-dependent inference network $q_\phi(\mathbf{z}_t | \mathbf{x}_{1:t})$ that approximates it with a conditional Gaussian distribution $\mathcal{N}(\mu_\phi(\mathbf{x}_{1:t}), \sigma_\phi(\mathbf{x}_{1:t}))$. The model is trained by optimizing the variational lower bound:

$$\mathcal{L}_{\theta, \phi}(\mathbf{x}_{1:T}) = \sum_{t=1}^T [\mathbb{E}_{q_\phi(\mathbf{z}_{1:t} | \mathbf{x}_{1:t})} \log p_\theta(\mathbf{x}_t | \mathbf{x}_{1:t-1}, \mathbf{z}_{1:t}) - \beta D_{KL}(q_\phi(\mathbf{z}_t | \mathbf{x}_{1:t}) || p(\mathbf{z}))]$$

Given the form of p_θ the likelihood term reduces to an ℓ_2 penalty between $\hat{\mathbf{x}}_t$ and \mathbf{x}_t . We train the model using the re-parameterization trick (Kingma & Welling, 2014) and by estimating the expectation over $q_\phi(\mathbf{z}_{1:t} | \mathbf{x}_{1:t})$ with a single sample. See Appendix A for a full derivation of the loss.

The hyper-parameter β represents the trade-off between minimizing frame prediction error and fitting the prior. A smaller β increases the capacity of the inference network. If β is too small the inference network may learn to simply copy the target frame \mathbf{x}_t , resulting in low prediction error during training but poor performance at test time due to the mismatch between the posterior $q_\phi(\mathbf{z}_t | \mathbf{x}_{1:t})$ and the prior $p(\mathbf{z}_t)$. If β is too large, the model may under-utilize or completely ignore latent variables \mathbf{z}_t and reduce to a deterministic predictor. In practice, we found β easy to tune, particularly for the learned-prior variant we discuss below. For a discussion of hyperparameter β in the context of variational autoencoders see Higgins et al. (2017).

Fixed prior: The simplest choice for $p(\mathbf{z}_t)$ is a fixed Gaussian $\mathcal{N}(0, \mathbf{I})$, as is typically used in variational auto encoder models. We refer to this as the SVG-FP model, as shown in Fig. 2a. A drawback is that samples at each time step

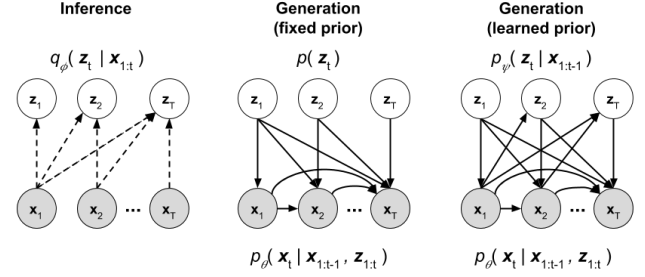


Figure 1. Inference (left) and generation in the SVG-FP (middle) and SVG-LP models (right).

will be drawn randomly, thus ignore temporal dependencies present between frames.

Learned prior: A more sophisticated approach is to learn a prior that varies across time, being a function of all past frames up to *but not including* the frame being predicted $p_\psi(\mathbf{z}_t | \mathbf{x}_{1:t-1})$. Specifically, at time t a prior network observes frames $\mathbf{x}_{1:t-1}$ and output the parameters of a conditional Gaussian distribution $\mathcal{N}(\mu_\psi(\mathbf{x}_{1:t-1}), \sigma_\psi(\mathbf{x}_{1:t-1}))$. The prior network is trained jointly with the rest of the model by maximizing:

$$\mathcal{L}_{\theta, \phi, \psi}(\mathbf{x}_{1:T}) = \sum_{t=1}^T [\mathbb{E}_{q_\phi(\mathbf{z}_{1:t} | \mathbf{x}_{1:t})} \log p_\theta(\mathbf{x}_t | \mathbf{x}_{1:t-1}, \mathbf{z}_{1:t}) - \beta D_{KL}(q_\phi(\mathbf{z}_t | \mathbf{x}_{1:t}) || p_\psi(\mathbf{z}_t | \mathbf{x}_{1:t-1}))]$$

We refer to this model as SVG-LP and illustrate the training procedure in Fig. 2b.

At test time, a frame at time t is generated by first sampling \mathbf{z}_t from the prior. In SVG-FP we draw $\mathbf{z}_t \sim \mathcal{N}(0, \mathbf{I})$ and in SVG-LP we draw $\mathbf{z}_t \sim p_\psi(\mathbf{z}_t | \mathbf{x}_{1:t-1})$. Then, a frame is generated by $\hat{\mathbf{x}}_t = \mu_\theta(\mathbf{x}_{1:t-1}, \mathbf{z}_{1:t})$. After conditioning on a short series of real frames, the model begins to pass generated frames $\hat{\mathbf{x}}_t$ back into the input of the prediction model and, in the case of the SVG-LP model, the prior. The sampling procedure for SVG-LP is illustrated in Fig. 2c.

Architectures: We use a generic convolutional LSTM for p_θ , q_ϕ and p_ψ . Frames are input to the LSTMs via a feed-forward convolutional network, shared across all three parts of the model. A convolutional frame decoder maps the output of the frame predictor’s recurrent network back to pixel space.

For a time step t during training, the generation is as follows, where the LSTM recurrence is omitted for brevity:

$$\begin{aligned} \mu_\phi(t), \sigma_\phi(t) &= LSTM_\phi(h_t) & h_t &= Enc(\mathbf{x}_t) \\ \mathbf{z}_t &\sim \mathcal{N}(\mu_\phi(t), \sigma_\phi(t)) \\ g_t &= LSTM_\theta(h_{t-1}, \mathbf{z}_t) & h_{t-1} &= Enc(\mathbf{x}_{t-1}) \\ \mu_\theta(t) &= Dec(g_t) \end{aligned}$$

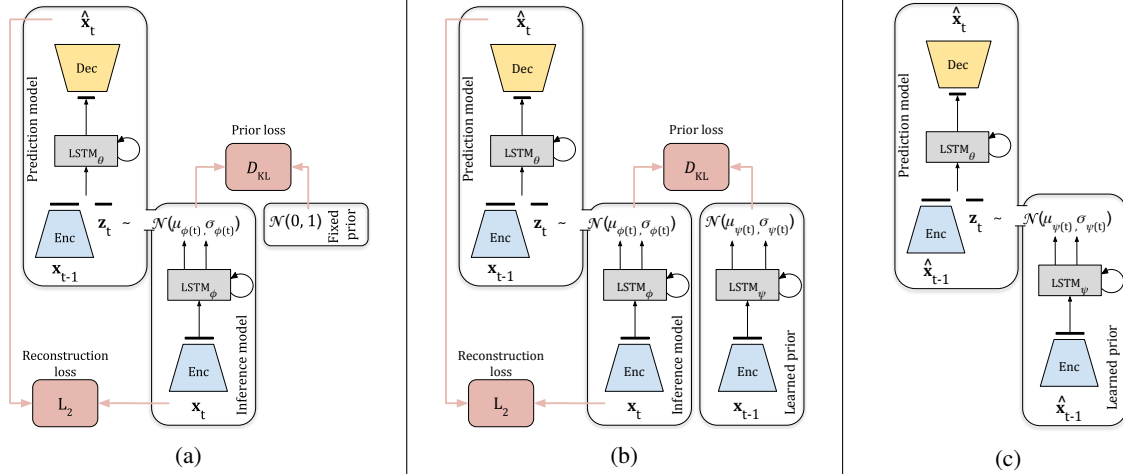


Figure 2. Our proposed video generation model. (a) Training with a fixed prior (SVG-FP); (b) Training with learned prior (SVG-LP); (c) Generation with the learned prior model. The red boxes show the loss functions used during training. See text for details.

During training, the parameters of the encoder *Enc* and decoder *Dec* are also learned, along with the rest of the model, in an end-to-end fashion (we omit their parameters from the loss functions above for brevity).

In the learned-prior model (SVG-LP), the parameters of the prior distribution at time t are generated as follows, where the LSTM recurrence is omitted for brevity:

$$\begin{aligned} h_{t-1} &= \text{Enc}(\mathbf{x}_{t-1}) \\ \mu_\psi(t), \sigma_\psi(t) &= \text{LSTM}_\psi(h_{t-1}) \end{aligned}$$

3.1. Discussion of related models

Our model is related to a recent stochastic variational video prediction model of Babaeizadeh et al. (2017). Although their variational framework is broadly similar, a key difference between this work and ours is the way in which the latent variables \mathbf{z}_t are estimated during training and sampled at test time.

The inference network of Babaeizadeh et al. (2017) encodes the *entire video sequence* via a feed forward convolutional network to estimate $q_\theta(\mathbf{z}|\mathbf{x}_{1:T})$. They propose two different models that use this distribution. In the time-invariant version, a single \mathbf{z} is sampled for the entire video sequence. In the time-variant model, a different $\mathbf{z}_t \sim q_\theta(\mathbf{z}|\mathbf{x}_{1:T})$ is sampled for every time step, all samples coming from the *same distribution*.

In contrast, both our fixed-prior and learned-prior models utilize a more flexible inference network that outputs a different posterior distribution for every time step given by $q_\theta(\mathbf{z}_t|\mathbf{x}_{1:t})$ (note $\mathbf{x}_{1:t}$, not $\mathbf{x}_{1:T}$ as above).

At test time, our fixed-prior model and the time-variant model of Babaeizadeh et al. (2017) sample \mathbf{z}_t from a fixed

Gaussian prior at every time step. By contrast, our learned-prior model draws samples from the time-varying distribution: $p_\psi(\mathbf{z}_t|\mathbf{x}_{1:t-1})$, whose parameters ψ were estimated during training.

These differences manifest themselves in two ways. First, the generated frames are significantly sharper with both our models (see direct comparisons to Babaeizadeh et al. (2017) in Figure Fig. 9). Second, training our model is much easier. Despite the same *prior* distribution being used for both our fixed-prior model and Babaeizadeh et al. (2017), the time variant *posterior* distribution introduced in our model appears crucial for successfully training the model. Indeed, Babaeizadeh et al. (2017) report difficulties training their model by naively optimizing the variational lower bound, noting that the model simply ignores the latent variables. Instead, they propose a scheduled three phase training procedure whereby first the deterministic element of the model is trained, then latent variables are introduced but the KL loss is turned off and in the final stage the model is trained with the full loss. In contrast, both our fixed-prior and learned-prior models are easily trainable end-to-end in a single phase using a unified loss function.

4. Experiments

We evaluate our SVG-FP and SVG-LP model on one synthetic video dataset (Stochastic Moving MNIST) and two real ones (KTH actions (Schuldt et al., 2004) and BAIR robot (Ebert et al., 2017)). We show quantitative comparisons by computing structural similarity (SSIM) and Peak Signal-to-Noise Ratio (PSNR) scores between ground truth and generated video sequences. Since neither of these metrics fully captures perceptual fidelity of generated sequences we also make a qualitative comparison between samples

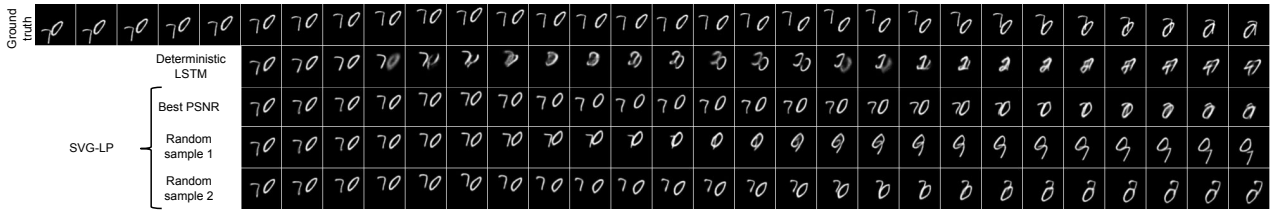


Figure 3. Qualitative comparison between SVG-LP and a purely deterministic baseline. The deterministic model produces sharp predictions until ones of the digits collides with a wall, at which point the prediction blurs to account for the many possible futures. In contrast, samples from SVG-LP show the digit bouncing off in different plausible directions.

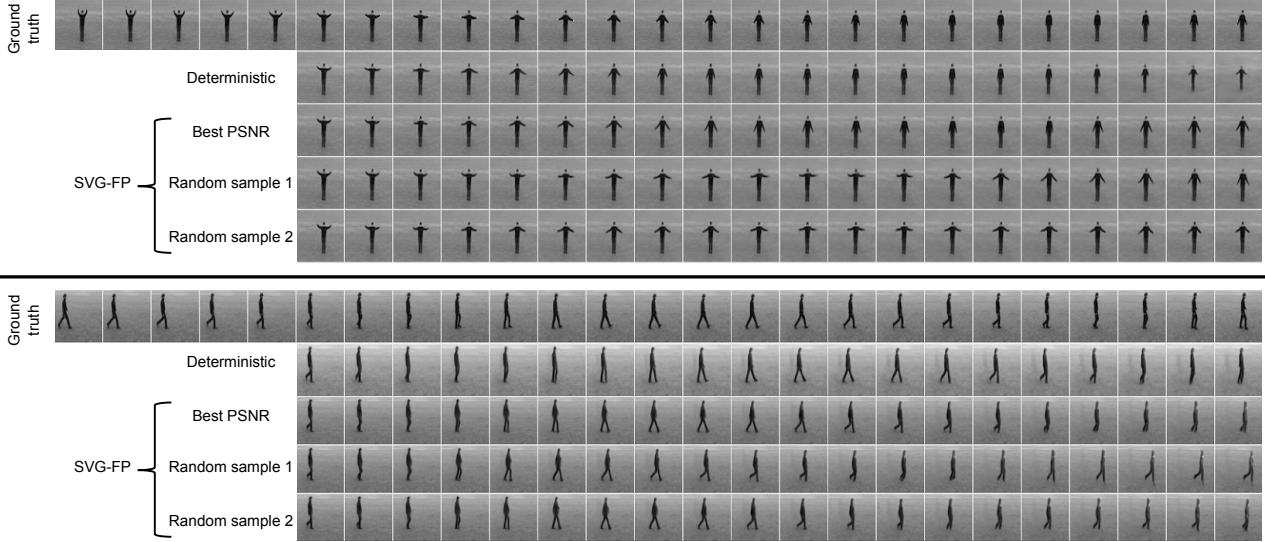


Figure 4. Qualitative comparison between SVG-LP and a purely deterministic baseline. Both models were conditioned on the first 10 frames (the final 5 are shown in the figure) of test sequences. The deterministic model produces plausible predictions for the future frames but frequently mispredicts precise limb locations. In contrast, different samples from SVG-FP reflect the variability on the persons pose in future frames. By picking the sample with the best PSNR, SVG-FP closely matches the ground truth sequence.

from our model and current state-of-the-art methods. We encourage the reader to view additional generated videos at: <https://sites.google.com/view/svglp/>.

4.1. Model architectures

$LSTM_\theta$ is a two layer LSTMs with 256 cells in each layer. $LSTM_\phi$ and $LSTM_\psi$ are both single layer LSTMs with 256 cells in each layer. Each network has a linear embedding layer and a fully connected output layer. The output of $LSTM_\theta$ is passed through a tanh nonlinearity before going into the frame decoder.

For Stochastic Moving MNIST, the frame encoder has a DCGAN discriminator architecture (Radford et al., 2016) with output dimensionality $|h| = 128$. Similarly, the decoder uses a DCGAN generator architecture and a sigmoid output layer. The output dimensionalities of the LSTM networks are $|g| = 128$, $|\mu_\phi| = |\mu_\psi| = 10$.

For KTH and BAIR datasets, the frame encoder uses the same architecture as VGG16 (Simonyan & Zisserman, 2015) up until the final pooling layer with output dimensionality $|h| = 128$. The decoder is a mirrored version of the encoder with pooling layers replaced with spatial up-sampling and a sigmoid output layer. The output dimensionalities of the LSTM networks are $|g| = 128, |\mu_\phi| = |\mu_\psi| = 32$ for KTH and $|g| = 128, |\mu_\phi| = |\mu_\psi| = 64$ for BAIR.

For all datasets we add skip connections from the encoder at the last ground truth frame to the decoder at t , enabling the model to easily generate static background features.

We also train a deterministic baseline with the same encoder, decoder and LSTM architecture as our frame predictor p_θ but with the latent variables omitted.

We train all the models with the ADAM optimizer (Kingma & Ba, 2014) and learning rate $\eta = 0.002$. We set $\beta = 1\text{e-}4$ for KTH and BAIR and $\beta = 1\text{e-}6$ for KTH. Source code and

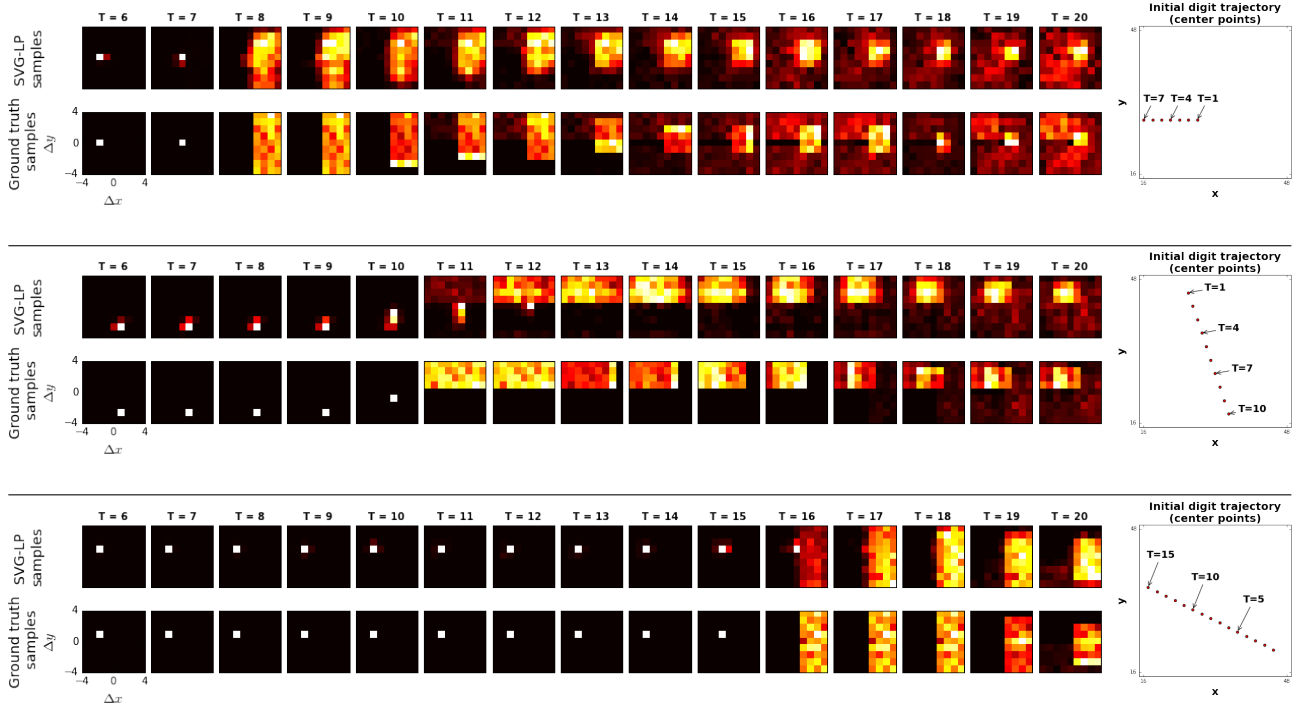


Figure 5. Three examples of our SVG-LP model accurately capturing the distribution of MNIST digit trajectories following collision with a wall. On the right we show the trajectory of a digit prior to the collision. In the ground truth sequence, the angle and speed immediately after impact are drawn from at random from uniform distributions. Each of the sub-plots shows the *distribution* of $\Delta x, \Delta y$ at each time step. In the lower ground truth sequence, the trajectory is deterministic before the collision (occurring between $t = 7$ and $t = 8$ in the first example), corresponding to a delta-function. Following the collision, the distribution broadens out to an approximate uniform distribution (e.g. $t = 8$), before being reshaped by subsequent collisions. The upper row shows the distribution estimated by our SVG-LP model (after conditioning on ground-truth frames from $t = 1 \dots 5$). Note how our model accurately captures the correct distribution many time steps into the future, despite its complex shape. The distribution was computed by drawing many samples from the model, as well as averaging over different digits sharing the same trajectory. The 2nd and 3rd examples show different trajectories with correspondingly different impact times ($t = 11$ and $t = 16$ respectively).

trained models are available at <https://github.com/edenton/svg>.

4.2. Stochastic Moving MNIST

We introduce the Stochastic Moving MNIST (SM-MNIST) dataset which consists of sequences of frames of size 64×64 , containing one or two MNIST digits moving and bouncing off edge of the frame (walls). In the original Moving MNIST dataset (Srivastava et al., 2015) the digits move with constant velocity and bounce off the walls in a deterministic manner. By contrast, SM-MNIST digits move with a constant velocity along a trajectory until they hit at wall at which point they bounce off with a random speed and direction. This dataset thus contains segments of deterministic motion interspersed with moments of uncertainty, i.e. each time a digit hits a wall.

Training sequences were generated on the fly by sampling two different MNIST digits from the training set (60k total digits) and two distinct trajectories. Trajectories were con-

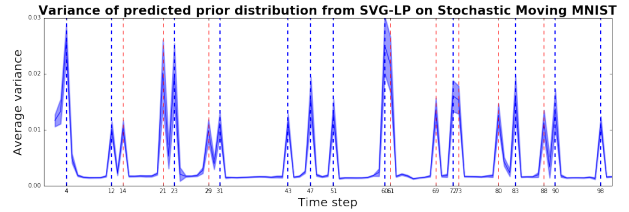


Figure 6. Learned prior of SVG-LP accurately predicts collision points in SM-MNIST. Five hundred test video sequences with different MNIST test digits but synchronized motion were fed into the learned prior. The mean (\pm one standard deviation) of $\sigma_{\psi}(\mathbf{x}_{1:t-1})$ is plotted for $t = 1, \dots, 100$. The true points of uncertainty in the video sequences, i.e. when a digit hits a wall, are marked by vertical lines, colored red and blue for each digit respectively.

structed by uniformly sampling (x, y) starting locations and initial velocity vectors $(\Delta x, \Delta y) \in [-4, 4] \times [-4, 4]$. Every time a digit hits a wall a new velocity vector is sampled.

We trained our SVG models and a deterministic baseline

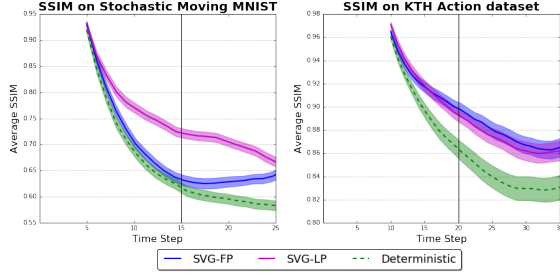


Figure 7. Quantitative evaluation of SVG-FP and SVG-LP video generation quality on SM-MNIST (left) and KTH (right). The models are conditioned on the first 5 frames for SM-MNIST and 10 frames for KTH. The vertical bar indicates the frame number the models were trained to predict up to; further generations indicate generalization ability. Mean SSIM over test videos is plotted with 95% confidence interval shaded.

on SM-MNIST by conditioning on 5 frames and training the model to predict the next 10 frames in the sequence. We compute SSIM for SVG-FP and SVG-LP by drawing 100 samples from the model for each test sequence and picking the one with the best score with respect to the ground truth. Fig. 7(left) plots average SSIM on unseen test videos. Both SVG-FP and SVG-LP outperform the deterministic baseline and SVG-LP performs best overall, particularly in later time steps. Fig. 3 shows sample generations from the deterministic model and SVG-LP. Generations from the deterministic model are sharp for several time steps, but the model rapidly degrades after a digit collides with the wall, since the subsequent trajectory is uncertain.

We hypothesize that the improvement of SVG-LP over the SVG-FP model is due to the mix of deterministic and stochastic movement in the dataset. In SVG-FP, the frame predictor must determine how and if the latent variables for a given time step should be integrated into the prediction. In SVG-LP, the burden of predicting points of high uncertainty can be offloaded to the prior network.

Empirically, we measure this in Fig. 6. Five hundred different video sequences were constructed, each with different test digits, but whose trajectories were synchronized. The plot shows the mean of $\sigma_\psi(\mathbf{x}_{1:t})$, i.e., the variance of the distribution over \mathbf{z}_t predicted by the learned prior over 100 time steps. Superimposed in red and blue are the time instants when the respective digits hit a wall. We see that the learned prior is able to accurately predict these collisions that result in significant randomness in the trajectory.

One major challenge when evaluating generative video models is assessing how accurately they capture the full distribution of possible outcomes, mainly due to the high dimensionality of the space in which samples are drawn. However, the synthetic nature of single digit SM-MNIST allows us to investigate this in a principled way. A key point to note is

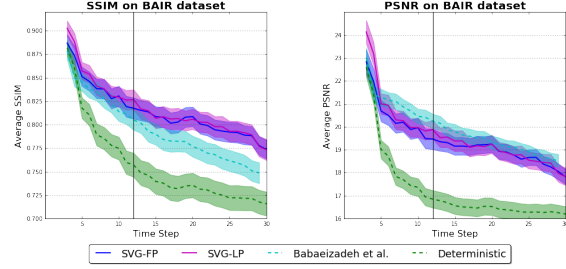


Figure 8. Quantitative comparison between our SVG models and Babaeizadeh et al. (2017) on the BAIR robot dataset. All models are conditioned on the first two frames and generate the subsequent 28 frames. The models were trained to predict up to 10 frames in the future, indicated by the vertical bar; further generations indicate generalization ability. Mean SSIM and PSNR over test videos is plotted with 95% confidence interval shaded.

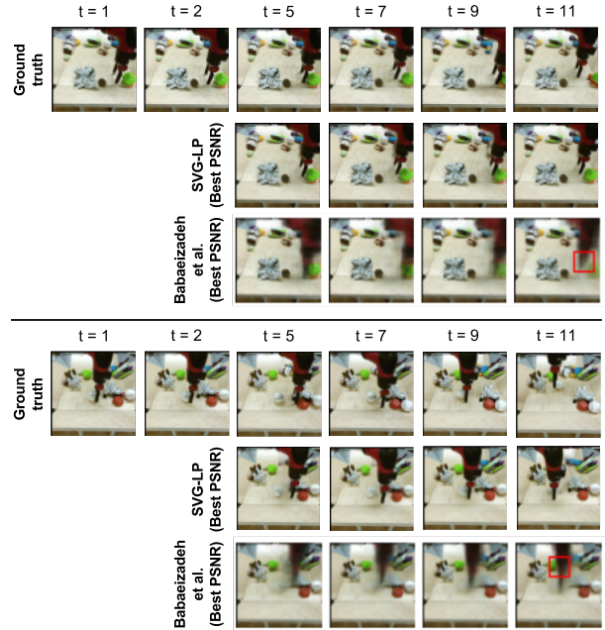


Figure 9. Qualitative comparison between our SVG-LP model and Babaeizadeh et al. (2017). All models are conditioned on the first two frames of unseen test videos. SVG-LP generates crisper images and predicts plausible movement of the robot arm.

that with each sequence, the digit appearance remains constant with the only randomness coming from its trajectory once it hits the image boundary. Thus for a sequence generated from our model, we can establish the digit trajectory by taking a pair of frames at any time step and cross-correlating them with the digit used in the initial conditioning frames. Maxima in each frame reveal the location of the digit, and the difference between the two gives us the velocity vector at that time. By taking an expectation over many samples from our model (also using the same trajectory but different digits), we can compute the empirical distribution of

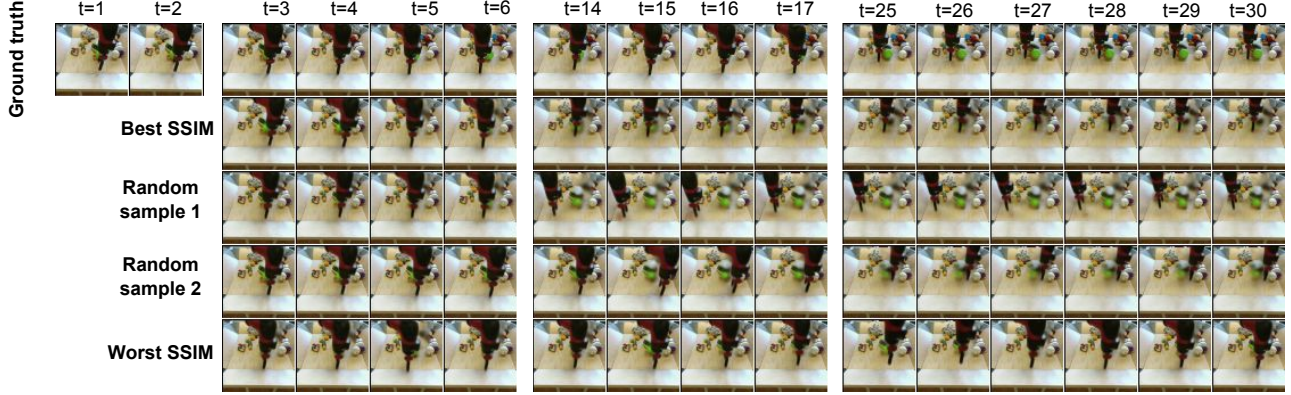


Figure 10. Additional examples of generations from SVG-LP showing crisp and varied predictions. A large segment of the background is occluded in conditioning frames, preventing SVG-LP from directly copying these background pixels into generated frames. In addition to crisp robot arm movement, SVG-LP generates plausible background objects in the space occluded by the robot arm in initial frames.

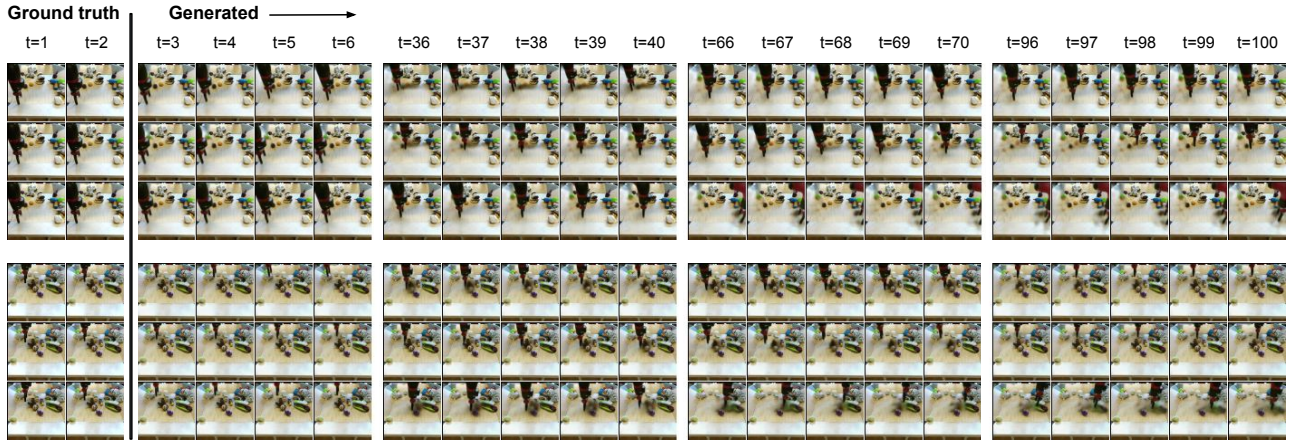


Figure 11. Long range generations from SVG-LP. The robot arm remains crisp up to 100 time steps and object motion can be seen in the generated video frames. Additional videos can be viewed at: <https://sites.google.com/view/svglp/>.

trajectories produced by our model. We can then perform the same operation on a validation set of ground truth sequences, to produce the true distribution of digit trajectories and compare it to the one produced by our model.

Fig. 5 shows SVG-LP (trained on *single* digit SM-MNIST) accurately capturing the distribution of MNIST digit trajectories for many time steps. The digit trajectory is deterministic before a collision. This is accurately reflected by the highly peaked distribution of velocity vectors from SVG-LP in the time steps leading up to a collision. Following a collision, the distribution broadens to approximately uniform before being reshaped by subsequent collisions. Crucially, SVG-LP accurately captures this complex behavior for many time steps. The temporally varying nature of the true trajectory distributions further supports the need for a learned prior $p_{\psi}(\mathbf{z}_t | \mathbf{x}_{1:t-1})$.

4.3. KTH Action Dataset

The KTH Action dataset (Schuldt et al., 2004) consists of real-world videos of people performing one of six actions (walking, jogging, running, boxing, handwaving, handclapping) against fairly uniform backgrounds. The human motion in the video sequences is fairly regular, however there is still uncertainty regarding the precise locations of the person’s joints at subsequent time steps. We trained SVG-FP, SVG-LP and the deterministic baseline on 64×64 video sequences by conditioning on 10 frames and training the model to predict the next 10 frames in the sequence.

We compute SSIM for SVG-FP and SVG-LP by drawing 100 samples from the model for each test sequence and picking the one with the best score with respect to the ground truth. Fig. 7(right) plots average SSIM on unseen test videos. SVG-FP and SVG-LP perform comparably on this dataset and both outperform the deterministic baseline. Fig. 4 shows

generations from the deterministic baseline and SVG-FP. The deterministic model predicts plausible future frames but, due to the inherent uncertainty in precise limb locations, often deviates from the ground truth. In contrast, different samples from the stochastic model reflect the variability in future frames indicating the latent variables are being utilized even on this simple dataset.

4.4. BAIR robot pushing dataset

The BAIR robot pushing dataset (Ebert et al., 2017) contains videos of a Sawyer robotic arm pushing a variety of objects around a table top. The movements of the arm are highly stochastic, providing a good test for our model. Although the dataset does contain actions given to the arm, we discard them during training and make frame predictions based solely on the video input.

Following Babaeizadeh et al. (2017), we train SVG-FP, SVG-LP and the deterministic baseline by conditioning on the first two frames of a sequence and predicting the subsequent 10 frames. We compute SSIM for SVG-FP and SVG-LP by drawing 100 samples from the model for each test sequence and picking the one with the best score with respect to the ground truth. Fig. 8 plots average SSIM and PSNR scores on 256 held out test sequences, comparing to the state-of-the-art approach of Babaeizadeh et al. (2017). This evaluation consists of conditioning on 2 frames and generating 28 subsequent ones, i.e. longer than at train time, demonstrating the generalization capability of SVG-FP and SVG-LP. Both SVG-FP and SVG-LP outperform Babaeizadeh et al. (2017) in terms of SSIM. SVG-LP outperforms the remaining models in terms of PSNR for the first few steps, after which Babaeizadeh et al. (2017) is marginally better. Qualitatively, SVG-FP and SVG-LP produce significantly sharper generations than Babaeizadeh et al. (2017), as illustrated in Fig. 9. PSNR is biased towards overly smooth (i.e. blurry) results which might explain the slightly better PSNR scores obtained by Babaeizadeh et al. (2017) for later time steps.

SVG-FP and SVG-LP produce crisp generations many time steps into the future. Fig. 10 shows sample generations up to 30 time steps alongside the ground truth video frames. We also ran SVG-LP forward for 100 time steps and continue to see crisp motion of the robot arm (see Fig. 11).

5. Discussion

We have introduced a novel video prediction model that combines a deterministic prediction of the next frame with stochastic latent variables, drawn from a time-varying distribution learned from training sequences. Our recurrent inference network estimates the latent distribution for each time step allowing easy end-to-end training. Evaluating

the model on real-world sequences, we demonstrate high quality generations that are comparable to, or better than, existing approaches. On synthetic data where it is possible to characterize the distribution of samples, we see that is able to match complex distributions of futures. The framework is sufficiently general that it can readily be applied to more complex datasets, given appropriate encoder and decoder modules.

Acknowledgements

Emily Denton is grateful for the support of a Google PhD fellowship. This work was supported by ONR #N00014-13-1-0646 and an NSF CAREER grant.

References

- Agrawal, P, Carreira, J, and Malik, J. Learning to see by moving. In *Proceedings of the International Conference on Computer Vision (ICCV)*, 2015.
- Babaeizadeh, Mohammad, Finn, Chelsea, Erhan, Dumitru, Campbell, Roy H., and Levine, Sergey. Stochastic variational video prediction. *arXiv:1710.11252*, 2017.
- Bayer, Justin and Osendorfer, Christian. Learning stochastic recurrent networks. *arXiv:1411.7610*, 2014.
- Bowman, Samuel R., Vilnis, Luke, Vinyals, Oriol, Dai, Andrew M., Jozefowicz, Rafal, and Bengio, Samy. Generating sentences from a continuous space. In *Proceedings of The SIGNLL Conference on Computational Natural Language Learning (CoNLL)*, 2016.
- Chiappa, S., Racaniere, S., Wierstra, D., and Mohamed, S. Recurrent environment simulators. In *Proceedings of the International Conference on Learning Representations (ICLR)*, 2017.
- Chung, Junyoung, Kastner, Kyle, Dinh, Laurent, Goel, Kratharth, Courville, Aaron, and Bengio, Yoshua. A recurrent latent variable model for sequential data. In *Advances in Neural Information Processing Systems (NIPS)*, 2015.
- Denton, Remi and Birodkar, Vighnesh. Unsupervised learning of disentangled representations from video. In *Advances in Neural Information Processing Systems (NIPS)*, 2017.
- Ebert, Frederik, Finn, Chelsea, Lee, Alex X., and Levine, Sergey. Self-supervised visual planning with temporal skip connections. In *Conference on Robot Learning (CoRL)*, 2017.
- Finn, C., Goodfellow, I., and Levine, S. Unsupervised learning for physical interaction through video prediction. In *Advances in Neural Information Processing Systems (NIPS)*, 2016.

- Fraccaro, Marco, Snderby, Sren Kaae, Paquet, Ulrich, and Winther, Ole. Sequential neural models with stochastic layers. In *Advances in Neural Information Processing Systems (NIPS)*, 2016.
- Goodfellow, Ian J., Pouget-Abadie, Jean, Mirza, Mehdi, Xu, Bing, Warde-Farley, David, Ozair, Sherjil, Courville, Aaron, and Bengio, Yoshua. Generative adversarial nets. In *Advances in Neural Information Processing Systems (NIPS)*, 2014.
- Goroshin, Ross, Mathieu, Michael, and LeCun, Yann. Learning to linearize under uncertainty. In *Advances in Neural Information Processing Systems 28*, 2015.
- Henaff, Mikael, Zhao, Junbo, and LeCun, Yann. Prediction under uncertainty with error-encoding networks. *arXiv:1711.04994*, 2017.
- Higgins, Irina, Matthey, Loic, Pal, Arka, Burgess, Christopher, Glorot, Xavier, Botvinick, Matthew, Mohamed, Shakir, and Lerchner, Alexander. Early visual concept learning with unsupervised deep learning. In *Proceedings of the International Conference on Learning Representations (ICLR)*, 2017.
- Jayaraman, D. and Grauman, K. Learning image representations tied to ego-motion. In *International Conference on Computer Vision*, 2015.
- Kalchbrenner, N., van den Oord, A., Simonyan, K., Danihelka, I., Vinyals, O., Graves, A., and Kavukcuoglu, K. Video pixel networks. *arXiv:1610.00527*, 2016.
- Karras, Tero, Aila, Timo, Laine, Samuli, and Lehtinen, Jaakko. Progressive growing of gans for improved quality, stability, and variation. *arXiv:1710.10196*, 2017.
- Kingma, Diederik and Ba, Jimmy. Adam: A method for stochastic optimization. *Proceedings of the International Conference on Learning Representations (ICLR)*, 2014.
- Kingma, D.P. and Welling, M. Auto-encoding variational bayes. In *Proceedings of the International Conference on Learning Representations (ICLR)*, 2014.
- Krishnan, R., Shalit, U., and Sontag, D. Deep kalman filters. *arXiv:1511.05121*, 2015.
- Liu, C. Beyond pixels: exploring new representations and applications for motion analysis. *PhD thesis, Massachusetts Institute of Technology*, 2009.
- Lotter, William, Kreiman, Gabriel, and Cox, David. Deep predictive coding networks for video prediction and unsupervised learning. *arXiv:1605.08104*, 2016.
- Mathieu, Michaël, Couprie, Camille, and LeCun, Yann. Deep multi-scale video prediction beyond mean square error. In *Proceedings of the International Conference on Learning Representations (ICLR)*, 2016.
- Oh, J., Guo, X., Lee, H., Lewis, R., and Singh, S. Action-conditional video prediction using deep networks in Atari games. In *Advances in Neural Information Processing Systems (NIPS)*, 2015.
- Radford, Alec, Metz, Luke, and Chintala, Soumith. Unsupervised representation learning with deep convolutional generative adversarial networks. In *Proceedings of the International Conference on Learning Representations (ICLR)*, 2016.
- Ranzato, Marc’Aurelio, Szlam, Arthur, Bruna, Joan, Mathieu, Michaël, Collobert, Ronan, and Chopra, Sumit. Video (language) modeling: a baseline for generative models of natural videos. *arXiv 1412.6604*, 2014.
- Reed, Scott, van den Oord, Aaron, Kalchbrenner, Nal, Colmenarejo, Sergio Gomez, Wang, Ziyu, Belov, Dan, and de Freitas, Nando. Parallel multiscale autoregressive density estimation. In *Proceedings of the International Conference on Machine Learning (ICML)*, 2017.
- Salimans, Tim, Karpathy, Andrej, Chen, Xi, and Kingma, Diederik P. Pixelcnn++: Improving the pixelcnn with discretized logistic mixture likelihood and other modifications. *arXiv:1701.05517*, 2017.
- Schuldt, Christian, Laptev, Ivan, and Caputo, Barbara. Recognizing human actions: A local svm approach. In *Proceedings of the International Conference on Pattern Recognition*, 2004.
- Simonyan, K. and Zisserman, A. Very deep convolutional networks for large-scale image recognition. In *Proceedings of the International Conference on Learning Representations (ICLR)*, 2015.
- Sölch, Maximilian, Bayer, Justin, Ludersdorfer, Marvin, and van der Smagt, Patrick. Variational inference for online anomaly detection in high-dimensional time series. *arXiv:1602.07109*, 2016.
- Srivastava, N., Mansimov, E., and Salakhutdinov, R. Unsupervised learning of video representations using LSTMs. In *Proceedings of the International Conference on Machine Learning (ICML)*, 2015.
- van den Oord, A., Kalchbrenner, N., and Kavukcuoglu, K. Pixel recurrent neural networks. In *Proceedings of the International Conference on Machine Learning (ICML)*, 2016.

- Villegas, R., Yang, J., Hong, S., Lin, X., and Lee, H. Decomposing motion and content for natural video sequence prediction. In *Proceedings of the International Conference on Learning Representations (ICLR)*, 2017a.
- Villegas, Ruben, Yang, Jimei, Zou, Yuliang, Sohn, Sungryull, Lin, Xunyu, and Lee, Honglak. Learning to generate long-term future via hierarchical prediction. In *Proceedings of the International Conference on Machine Learning (ICML)*, 2017b.
- Vondrick, C. and Torralba, A. Generating the future with adversarial transformers. In *Proceedings of the 2011 IEEE Conference on Computer Vision and Pattern Recognition*, 2017.
- Vondrick, C., Pirsiaavash, H., and Torralba, A. Generating videos with scene dynamics. In *arXiv 1609.02612*, 2016.
- Walker, J., Gupta, A., and Hebert, M. Dense optical flow prediction from a static image. In *ICCV*, 2015.
- Wang, Xiaolong and Gupta, Abhinav. Unsupervised learning of visual representations using videos. In *CVPR*, pp. 2794–2802, 2015.
- Wiskott, L. and Sejnowski, T. Slow feature analysis: Unsupervised learning of invariance. *Neural Computation*, 14(4):715–770, 2002.
- Xue, Tianfan, Wu, Jiajun, Bouman, Katherine L, and Freeman, William T. Visual dynamics: Probabilistic future frame synthesis via cross convolutional networks. In *Advances in Neural Information Processing Systems (NIPS)*, 2016.
- Zou, W. Y., Zhu, S., Ng, A. Y., , and Yu., K. Deep learning of invariant features via simulated fixations in video. In *Advances in Neural Information Processing Systems (NIPS)*, 2012.

Appendix

A. Variational bound

We first review the variational lower bound on the data likelihood:

$$\begin{aligned}
 \log p_\theta(\mathbf{x}) &= \log \int_{\mathbf{z}} p_\theta(\mathbf{x}|\mathbf{z})p(\mathbf{z}) \\
 &= \log \int_{\mathbf{z}} p_\theta(\mathbf{x}|\mathbf{z})p(\mathbf{z}) \frac{q_\phi(\mathbf{z}|\mathbf{x})}{q_\phi(\mathbf{z}|\mathbf{x})} \\
 &= \log \mathbb{E}_{q_\phi(\mathbf{z}|\mathbf{x})} \frac{p_\theta(\mathbf{x}|\mathbf{z})p(\mathbf{z})}{q_\phi(\mathbf{z}|\mathbf{x})} \\
 &\geq \mathbb{E}_{q_\phi(\mathbf{z}|\mathbf{x})} \log \frac{p_\theta(\mathbf{x}|\mathbf{z})p(\mathbf{z})}{q_\phi(\mathbf{z}|\mathbf{x})} \\
 &= \mathbb{E}_{q_\phi(\mathbf{z}|\mathbf{x})} \log p_\theta(\mathbf{x}|\mathbf{z}) - \mathbb{E}_{q_\phi(\mathbf{z}|\mathbf{x})} \log \frac{q_\phi(\mathbf{z}|\mathbf{x})}{p(\mathbf{z})} \\
 &= \mathbb{E}_{q_\phi(\mathbf{z}|\mathbf{x})} \log p_\theta(\mathbf{x}|\mathbf{z}) - D_{KL}(q_\phi(\mathbf{z}|\mathbf{x})||p(\mathbf{z}))
 \end{aligned}$$

Recall that the SVG frame predictor is parameterized by a recurrent neural network. At each time step the model takes as input \mathbf{x}_{t-1} and \mathbf{z}_t and through the recurrence the model also depends on $\mathbf{x}_{1:t-2}$ and $\mathbf{z}_{1:t-1}$. Then, we can further simplify the bound with:

$$\begin{aligned}
 \log p_\theta(\mathbf{x}|\mathbf{z}) &= \log \prod_t p_\theta(\mathbf{x}_t|\mathbf{x}_{1:t-1}, \mathbf{z}_{1:T}) \\
 &= \sum_t \log p_\theta(\mathbf{x}_t|\mathbf{x}_{1:t-1}, \mathbf{z}_{1:t}, \cancel{\mathbf{z}_{t+1:T}}) \\
 &= \sum_t \log p_\theta(\mathbf{x}_t|\mathbf{x}_{1:t-1}, \mathbf{z}_{1:t})
 \end{aligned}$$

Recall, the inference network used by SVG-FP and SVG-LP is parameterized by a recurrent neural network that outputs a different distribution $q_\phi(\mathbf{z}_t|\mathbf{x}_{1:t})$ for every time step t . Let $\mathbf{z} = [\mathbf{z}_1, \dots, \mathbf{z}_T]$ denote the collection of latent variables across all time steps and $q_\phi(\mathbf{z}|\mathbf{x})$ denote the distribution over \mathbf{z} . Due to the independence across time, we have

$$q_\phi(\mathbf{z}|\mathbf{x}) = \prod_t q_\phi(\mathbf{z}_t|\mathbf{x}_{1:t})$$

The independence of $\mathbf{z}_1, \dots, \mathbf{z}_T$ allows the D_{KL} term of the

loss to be decomposed into individual time steps:

$$\begin{aligned}
 D_{KL}(q_\phi(\mathbf{z}|\mathbf{x})||p(\mathbf{z})) &= \int_{\mathbf{z}} q_\phi(\mathbf{z}|\mathbf{x}) \log \frac{q_\phi(\mathbf{z}|\mathbf{x})}{p(\mathbf{z})} \\
 &= \int_{\mathbf{z}_1} \dots \int_{\mathbf{z}_T} q_\phi(\mathbf{z}_1|\mathbf{x}_1) \dots q_\phi(\mathbf{z}_T|\mathbf{x}_{1:T}) \log \frac{q_\phi(\mathbf{z}_1|\mathbf{x}_1) \dots q_\phi(\mathbf{z}_T|\mathbf{x}_{1:T})}{p(\mathbf{z}_1) \dots p(\mathbf{z}_T)} \\
 &= \int_{\mathbf{z}_1} \dots \int_{\mathbf{z}_T} q_\phi(\mathbf{z}_1|\mathbf{x}_1) \dots q_\phi(\mathbf{z}_T|\mathbf{x}_{1:T}) \sum_t \log \frac{q_\phi(\mathbf{z}_t|\mathbf{x}_{1:t})}{p(\mathbf{z}_t)} \\
 &= \sum_t \int_{\mathbf{z}_1} \dots \int_{\mathbf{z}_T} q_\phi(\mathbf{z}_1|\mathbf{x}_1) \dots q_\phi(\mathbf{z}_T|\mathbf{x}_{1:T}) \log \frac{q_\phi(\mathbf{z}_t|\mathbf{x}_{1:t})}{p(\mathbf{z}_t)}
 \end{aligned}$$

And because $\int_x p(x) = 1$ this simplifies to:

$$\begin{aligned}
 &= \sum_t \int_{\mathbf{z}_t} q_\phi(\mathbf{z}_t|\mathbf{x}_{1:t}) \log \frac{q_\phi(\mathbf{z}_t|\mathbf{x}_{1:t})}{p(\mathbf{z}_t)} \\
 &= \sum_t D_{KL}(q_\phi(\mathbf{z}_t|\mathbf{x}_{1:t})||p(\mathbf{z}_t))
 \end{aligned}$$

Putting this all together we have:

$$\begin{aligned}
 \log p_\theta(\mathbf{x}) &\geq \mathcal{L}_{\theta, \phi}(\mathbf{x}_{1:T}) \\
 &= \mathbb{E}_{q_\phi(\mathbf{z}|\mathbf{x})} \log p_\theta(\mathbf{x}|\mathbf{z}) - D_{KL}(q_\phi(\mathbf{z}|\mathbf{x})||p(\mathbf{z})) \\
 &= \sum_t [\mathbb{E}_{q_\phi(\mathbf{z}_{1:t}|\mathbf{x}_{1:t})} \log p_\theta(\mathbf{x}_t|\mathbf{x}_{1:t-1}, \mathbf{z}_{1:t}) \\
 &\quad - D_{KL}(q_\phi(\mathbf{z}_t|\mathbf{x}_{1:t})||p(\mathbf{z}_t))]
 \end{aligned}$$